Reprinted from MONTHLY WEATHER REVIEW, Vol. 121, No. 2, February 1993
American Meteorological Society

Toward More Accurate Wave-Permeable Boundary Conditions

DALE R. DURRAN AND MING-JEN YANG

DONALD N. SLINN

RANDY G. BROWN

Toward More Accurate Wave-Permeable Boundary Conditions

DALE R. DURRAN AND MING-JEN YANG

Department of Atmospheric Sciences, University of Washington, Seattle, Washington

DONALD N. SLINN

Department of Mechanical Engineering, University of Washington, Seattle, Washington

RANDY G. BROWN

Department of Atmospheric Sciences, University of Washington, Seattle, Washington

(Manuscript received 26 March 1992, in final form 2 July 1992)

ABSTRACT

This paper investigates several fundamental aspects of wave-permeable, or "radiation," lateral boundary conditions. Orlanski (1976) proposed that approximate wave-permeable boundary conditions could be constructed by advecting disturbances out of the domain at a phase speed c^*, which was to be calculated from the values of the prognostic variable near the boundary. Rigorous justification for this approach is possible for one-dimensional shallow-water flow. It is shown, however, that the floating c^* approach gives poor results in the one-dimensional shallow-water problem because all accuracy in the c^* calculations is eventually destroyed by the positive feedback between errors in c^* and (initially small) errors in the prognostic fields at the boundary. Better results were achieved by using fixed values of c^*. In our test cases, an externally specified c^* could deviate from the true phase speed $U + c$ by 40%–60% and still yield better results than schemes in which c^* was calculated at the boundary.

In order to examine the effects of wave dispersion on the question of whether c^* should be fixed or calculated, tests were conducted with a two-level shallow-water model. Once again, the simulations with fixed c^* were distinctly superior to those in which c^* was calculated at the boundary. A reasonable, though nonoptimal, value for the fixed c^* was the phase speed of the fastest wave.

Wave dispersion is, however, not the only factor that makes it difficult to specify wave-permeable boundary conditions. Two-dimensional shallow-water waves are nondispersive, but their trace velocities along the x and y axes are functions of wavenumber. As a consequence, the simple radiation boundary condition appropriate for one-dimensional shallow-water flow is just an approximation for two-dimensional flow. Engquist and Majda (1977) developed improved boundary conditions for the two-dimensional problem by constructing approximate "one-way equations." In this paper, the approach of Engquist and Majda is used to construct second-order one-way wave equations for situations with nonzero mean flow. The new boundary condition is tested against several alternative schemes and found to give the best results. The new boundary condition is particularly recommended for situations where waves strike the boundary at nonnormal angles of incidence.

1. Introduction

Numerical simulations of localized atmospheric phenomena are usually performed over computational domains that represent only a small and somewhat arbitrary portion of the total atmosphere. In such circumstances, the lateral and upper boundaries of the computational domain do not coincide with true physical boundaries, and the mathematical and numerical conditions imposed at these boundaries are intended to mimic the presence of the surrounding fluid. The boundary conditions should, therefore, allow disturbances traveling outward from the interior of the domain to pass through the boundary without generating spurious reflections that propagate back toward the interior. Boundary conditions designed to minimize spurious backward reflection have been referred to as *open, wave-permeable,* or *radiation* boundary conditions. The terminology "radiation boundary condition" is due to Sommerfeld (1949, p. 189), who defined the *condition of radiation* as "the sources must be *sources,* not *sinks* of energy. The energy which is radiated from the sources must scatter to infinity; *no energy may be radiated from infinity into . . . the field.*"

Previous researchers (e.g., Pearson 1974; Orlanski 1976; Miller and Thorpe 1981; Raymond and Kuo 1984; Hedley and Yau 1988) have expressed the Sommerfeld radiation condition mathematically as

Corresponding author address: Dr. Dale R. Durran, Department of Atmospheric Sciences, AK-40, University of Washington, Seattle, WA 98195.

$$\frac{\partial \phi}{\partial t} + c^* \frac{\partial \phi}{\partial x} = 0, \tag{1}$$

where ϕ is an arbitrary prognostic variable, c^* is some effective phase speed, and (1) is applied at an x boundary. In the case of one-dimensional subcritical linearized shallow-water flow, (1) is a correct statement of the radiation condition provided that at the right boundary ($x \to \infty$), $c^* = U + c$, or at the left boundary ($x \to -\infty$), $c^* = U - c$. Here U is the basic-state flow velocity and c is the shallow-water phase speed. Equation (1) is not, however, a correct formulation of the Sommerfeld radiation condition for more general physical systems in which the x trace velocity[1] is a function of wavelength. If c^* is a function of wavelength and two waves of different scale are simultaneously present at the boundary, no value of c^* can be specified a priori that will allow (1) to transmit both waves without reflection. Nevertheless, (1) has been widely used as an approximate radiation condition, and much research has been devoted to the problem of choosing an optimal c^*.

One example, where c^* is a function of wavelength, is gravity-wave propagation in stratified flow. Pearson (1974) suggested that (1) may be used to radiate internal gravity waves in stratified flow by fixing c^* at the Doppler-shifted phase speed of the dominant vertical mode. As an alternative, Orlanski (1976) suggested calculating c^* at a point just inside the boundary from the relation

$$c^* = -\frac{\partial \phi / \partial t}{\partial \phi / \partial x}. \tag{2}$$

In subsequent studies Miller and Thorpe (1981) proposed a number of higher-order numerical approximations to (2), and Hedley and Yau (1988) suggested that c^* be initially calculated from (2), and then modified by a number of empirical criteria. One purpose of this paper is to reexamine the relative merits of specifying c^* or attempting to calculate it using some variant of (2).

Raymond and Kuo (1984) attempted to improve the representation of the Sommerfeld radiation condition for multidimensional flow by replacing (1) with

$$\frac{\partial \phi}{\partial t} + c_x^* \frac{\partial \phi}{\partial x} + c_y^* \frac{\partial \phi}{\partial y} = 0, \tag{3}$$

where x and y are the horizontal coordinates and c_x^* and c_y^* are empirically determined phase speeds parallel to the x and y coordinates. In general, this is still not an exact formulation of the Sommerfeld radiation condition, but it is notable in that improvement is not sought by adjusting c^* but by refining the differential equation applied at the boundary. More sophisticated techniques for the construction of approximate radiation boundary conditions have been proposed for the two-dimensional wave equation,

$$\frac{\partial^2 \phi}{\partial t^2} - c^2 \left(\frac{\partial^2 \phi}{\partial x^2} + \frac{\partial^2 \phi}{\partial y^2} \right) = 0, \tag{4}$$

by Engquist and Majda (1977). A second purpose of this paper is to apply Engquist and Majda's approach to two-dimensional shallow-water flow with a mean wind and to compare the performance of the Engquist and Majda method with several other schemes.

Most of the previous papers on wave-permeable boundary conditions have assumed that the best radiation boundary condition was the formulation that most closely matched a small domain simulation to that on a larger domain. While this may be a very good way to tune a boundary condition empirically for a given application, if the model is nonlinear, it is not necessarily the best way to assess the fidelity with which a numerical scheme approximates the true radiation condition. As formulated by Sommerfeld, the radiation condition is applied at infinity, and its imposition at the edge of a finite domain can introduce error since even perfect wave-permeable boundary conditions may be incapable of correctly mimicking the presence of the surrounding fluid. After a disturbance propagates through a truly wave-permeable boundary, the numerical solution loses all memory of the disturbance. Yet some outward-propagating finite-amplitude disturbances are capable of generating signals that travel back toward the center of the computational domain, and when these disturbances exit through the boundary of the computational domain, their subsequent influence on the numerical solution is lost. In such circumstances, the differences that may arise between small- and large-domain simulations cannot be attributed solely to defects in the numerical formulation of the radiation boundary condition.

An example of the inadequacy of the radiation boundary condition is provided by a series of nonlinear mountain-wave simulations in Durran and Klemp (1983, Fig. 6). A very deep sponge layer was employed at the top boundary (the depth of the sponge was 1.5 vertical wavelengths and at least one half the total depth of the numerical domain). The sponge worked well for small-amplitude flow, but when finite-amplitude waves were present at the top boundary, the solutions became sensitive to the location of the upper boundary. This sensitivity increased dramatically with increasing wave amplitude. The deep-domain simulations appeared to differ from those in shallow domains because downward-propagating waves were generated by wave–wave interactions in the upper part of the deep domain, and the subsequent influence of these nonlinearly generated waves was captured in the deep-domain solution but lost in the shallow-domain simulations. Deep con-

[1] The x trace velocity is the apparent phase speed at which a wave, propagating in an arbitrary direction, appears to translate parallel to the x axis.

vective cloud simulations provide another example where the documented sensitivity of the simulations to the specification of the lateral boundary condition (Clark 1979; Hedley and Yau 1988), or to the location of the lateral boundary (Fovell and Ogura 1988), may be less the consequence of poorly approximating the radiation boundary condition than the result of inadequately capturing important feedbacks on the convection arising through the nonlinear processes outside the numerical domain. If one tunes c^* (or some algorithm for the computation of c^*) to minimize the difference between convective cloud simulations performed using large and small domains, the result may not be the c^* that minimizes spurious reflection but rather the c^* producing a reflection most closely simulating the inward-propagating influence that may develop as the convective circulation interacts with the surrounding fluid.

Errors generated by a failure to incorporate inward-propagating signals generated by real physical processes outside the boundaries of the computational domain cannot be reduced without using nested grids or enlarging the domain. Such errors are not the primary concern of this paper, which concentrates on improving the permeability of the lateral boundaries to outgoing waves. In order to ensure that all signal propagation should properly be directed outward through the boundaries, this investigation will focus on linear wave propagation problems. The question of whether it is best to specify c^* or to compute it from (2) is examined in the context of one-dimensional shallow-water flow in section 2. The influence of wave dispersion on this question is investigated using a two-layer shallow-water model in section 3.

Wave dispersion is not the only factor that makes it impossible to specify a perfect value for c^* in meteorological models of three-dimensional continuously stratified flow. As discussed at the beginning of this introduction, (1) is generally not an exact radiation condition for problems with more than one spatial dimension. Techniques for improving the formulation of radiation boundary conditions in multidimensional flows are examined in the context of the two-dimensional shallow-water system in sections 4 and 5. The second-order Engquist and Majda boundary condition is extended to two-dimensional shallow-water problems with nonzero mean flow in section 4 and tested against several competing schemes in section 5. Section 6 contains the conclusions.

2. One-dimensional shallow-water flow

How well do Orlanski-type calculations estimate c^*? It is difficult to assess the accuracy of such calculations in stratified flows because the correct c^* [i.e., the value for which (1) becomes a true radiation condition] is usually an unknown function of space and time. In linearized one-dimensional shallow-water flow, however, the correct c^* is known. If U denotes the speed of the mean flow and $c^2 = gH$, c^* is just $U \pm c$, the Doppler-shifted phase speed of shallow-water gravity waves. As the first step of an investigation into the ability of approximate formulas to estimate an appropriate c^*, let us examine how such formulas perform as boundary conditions for a linearized shallow-water model. The finite-difference equations for this simple model are

$$\frac{u_{i+1/2}^{n+1} - u_{i+1/2}^{n-1}}{2\Delta t} + U\left(\frac{u_{i+3/2}^{n} - u_{i-1/2}^{n}}{2\Delta x}\right) + \frac{\eta_{i+1}^{n-1} - \eta_{i}^{n-1}}{\Delta x} = 0, \quad (5)$$

$$\frac{\eta_{i}^{n+1} - \eta_{i}^{n-1}}{2\Delta t} + U\left(\frac{\eta_{i+1}^{n} - \eta_{i-1}^{n}}{2\Delta x}\right) + c^2\left(\frac{u_{i+1/2}^{n+1} - u_{i-1/2}^{n+1}}{\Delta x}\right) = 0. \quad (6)$$

Here u is the perturbation horizontal velocity, η is g times the displacement of the free surface from its equilibrium level, and the notation u_i^n indicates the numerical approximation to u at the point $x = i\Delta x$, $t = n\Delta t$. The velocity and height variables are spatially staggered such that the edge of the domain coincides with the outermost velocity points. According to (5) and (6), all spatial differences are centered, the time discretization of the advection terms is leapfrog, and the pressure-gradient and divergence terms are integrated with forward–backward differencing (Mesinger and Arakawa 1976). The overall scheme is nondamping and stable when

$$\frac{\Delta t}{\Delta x}\left[|U| \sin k\Delta x + 2c \sin\left(\frac{k\Delta x}{2}\right)\right] < 1 \quad \text{for all} \quad k \leq \frac{\pi}{\Delta x}.$$

A sufficient (though somewhat loose) condition for stability is, therefore, $(|U| + 2c)\Delta t/\Delta x < 1$. At the initial time the velocity is zero and

$$\eta(x, 0) = g \sin^4(\pi x). \quad (7)$$

The solution is computed on the domain $0 \leq x \leq 4$ km, with $\Delta x = 80$ m, $\Delta t = 0.48$ s, $c = 40$ m s^{-1}, $U = 10$ m s^{-1}, and radiation boundaries at $x = 0$ and $x = 4$ km.

Three numerical approximations to the free-surface displacement at $t = 72$ s are displayed in Fig. 1. The solid curve shows a numerical solution computed using periodic boundary conditions on the larger domain $-8 \leq x \leq 12$ km. The large-domain solution may be considered free from boundary-condition errors, since the periodic domain is too large to allow any disturbance exiting the region $0 \leq x \leq 4$ km to reenter that region before $t = 320$ s. The long-dashed curve in Fig. 1 shows the result obtained using (1) with $c^* = U \pm c$ at the

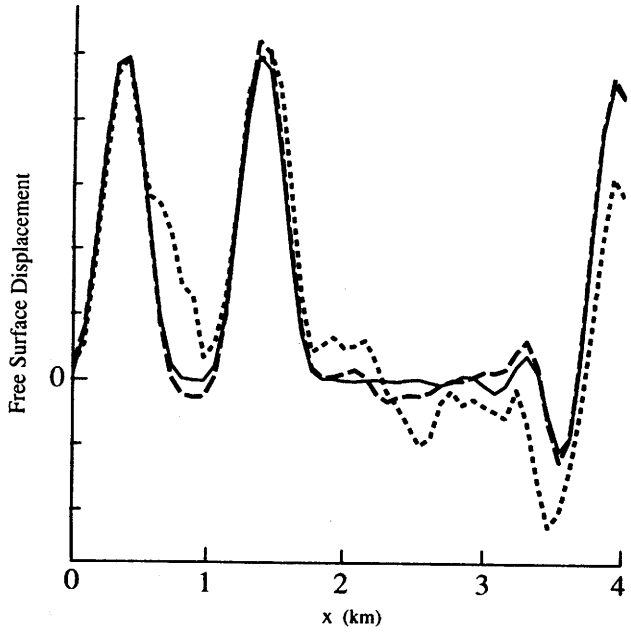

FIG. 1. Numerical solutions for the height field computed using periodic boundary conditions on a very large domain (solid line), and radiation boundary conditions with $c^* = U \pm \sqrt{gH}$ (long-dashed line) and c^* computed from the Orlanski condition (8) (short-dashed line).

appropriate inflow and outflow boundaries. This boundary condition is applied to each field using upstream differencing to step between time levels $t - \Delta t$ and $t + \Delta t$. The short-dashed curve shows the solution obtained by calculating c^* using Miller and Thorpe's (1981) formula

$$c^* = -\frac{\Delta x}{\Delta t}\left(\frac{\phi_{b-1}^{n} - \phi_{b-1}^{n-1}}{\phi_{b-1}^{n-1} - \phi_{b-2}^{n-1}}\right), \tag{8}$$

where ϕ represents either u or η, b is the index of the grid point at the right boundary, and the final value of c^* is constrained to lie in the interval $0 < c^* < 0.95\Delta x/2\Delta t$. (The preceding applies at the $x = 4$-km boundary; a similar expression is evaluated at $x = 0$.) This particular approximation to (2) was found to give better results than the original formula proposed by Orlanski (1976) or the higher-order variants suggested by Miller and Thorpe (1981). As one might expect, the solution obtained by specifying $c^* = U \pm c$ is superior to that obtained using the numerical calculation (8).[2] It is, however, somewhat surprising that the solution obtained by calculating c^* is so poor.

Suppose the gravity-wave phase speed is approximated by some constant value c_a and c^* is set to $U + c_a$ (or $U - c_a$) at the right (left) boundary. Even when c_a is a crude approximation to c, this approach can produce better results than those obtained by continually estimating c^* from (8). This superiority is illustrated in Fig. 2, in which the cumulative root-mean-square (rms) boundary-induced error is plotted as a function of c_a and compared with the error that develops when c^* is calculated using (8). The cumulative mean-square boundary-induced error in the solution is calculated as

$$E_1 = \frac{1}{2N_t}\sum_{n=1}^{N_t} \sigma_u(n) + \sigma_\eta(n), \tag{9}$$

where N_t is the total number of time steps and σ_u and σ_η are measures of the boundary-induced error in u and η. The boundary-induced error in a field ϕ at time n is computed according to the formula

$$\sigma_\phi^2(n) = \frac{\sum_{i=1}^{N_x} (\phi_i^n - \tilde{\phi}_i^n)^2}{\sum_{i=1}^{N_x} (\tilde{\phi}_i^n)^2}. \tag{10}$$

Here N_x is the number of spatial grid points and $\tilde{\phi}$ is the numerical solution computed using the large periodic domain. According to Fig. 2, the optimal choice of $c_a = c = 40$ m s^{-1} gives substantially less error than that generated by calculating c^* at the boundary. Moreover, fixed values of c_a are superior for $25 \leq c_a \leq 65$ m s^{-1}, or equivalently for $0.62c \leq c_a \leq 1.62c$. Consistent with the theoretical analysis of Klemp and

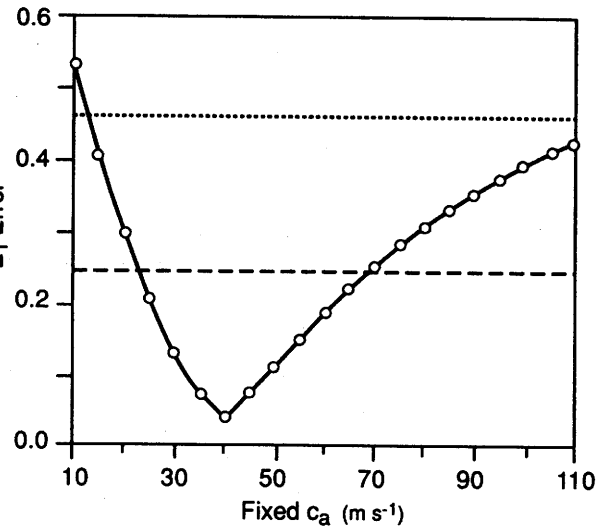

FIG. 2. Cumulative rms boundary-induced error after 200 time steps (E_1) generated by the misspecification of c^* as $U \pm c_a$, plotted as a function of c_a (solid curve). Also shown is the error for two variants of the Orlanski scheme that, being independent of c_a, appears as horizontal lines. The result using Orlanski's original formula for c^* is shown as the short-dashed line; the long-dashed line is obtained by computing c^* from (8).

[2] The $c^* = U \pm c$ solution does not perfectly match the large-domain periodic solution because of the one-sided differencing at the boundaries.

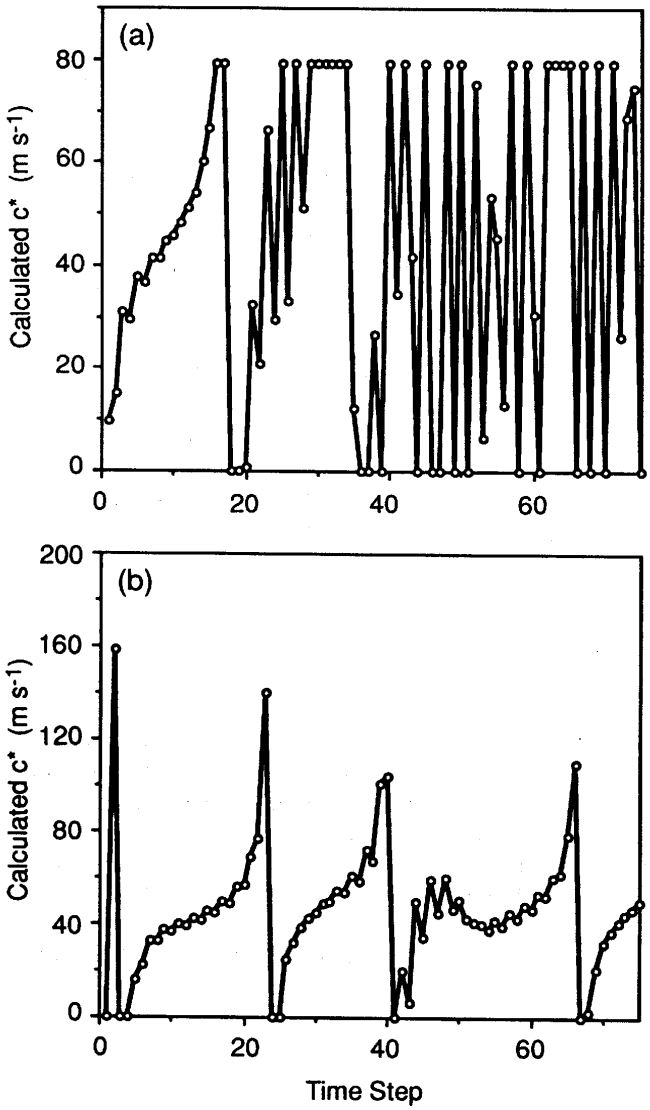

FIG. 3. Plot of c^* as a function of time step as calculated from the Orlanski scheme (8) using (a) the solution on the limited-domain and (b) the wide-domain periodic solution.

Lilly (1978), the asymmetry of the error about $c^* = c$ suggests that it is better to overestimate c_a than to underestimate it.

It is instructive to directly examine the c^* values calculated at the boundaries using the Orlanski-type approach. The right-hand boundary c^*, computed from (8), is plotted as a function of the time step in Fig. 3a. At the initial time, a wave trough is present at the boundary; every 20 time steps thereafter another trough or crest arrives at the boundary. During the interval between the passage of the initial trough and the first crest (the first 20 steps), the c^* calculation yields a somewhat reasonable approximation to the correct value of 50 m s^{-1}. During the interval between the passage of the first crest and the second trough (the second 20 steps), the computed c^* is quite noisy. After the first 40 steps, c^* is wildly over or underpredicted and repeatedly set to its limiting values of 0 or 80 m s^{-1} in an almost $2\Delta t$ oscillation. The most serious problem with the c^* calculation is not the fidelity with which the finite-difference approximation (8) approximates the continuous expression (2) but the susceptibility of the calculation to a positive feedback between the generation of error at the lateral boundary and further degradations in c^*. The effect of boundary-induced error on c^* may be appreciated by comparing Fig. 3a with Fig. 3b. Figure 3b shows the right-hand boundary c^* obtained when the large-domain periodic solution is substituted in (8). The results in Fig. 3b are much improved.[3] When c^* is diagnosed from the large-domain solution, there is no long-term trend in the error. The largest errors are associated with the passage of troughs or crests, in which case the denominator in (2) becomes small and the c^* calculation becomes very sensitive to numerical error.

The positive feedback between errors in c^* and errors in u and η is not surprising. The full equations support waves moving at both $U + c$ and $U - c$ and are not equivalent to (1). Thus, a computation such as (2) will not diagnose a meaningful phase speed unless one of these two admissable waves is absent. Very early in the simulation there are no inward-propagating waves at the lateral boundary and a reasonable calculation of c^* is possible (compare the first 20 steps in Figs. 3a and 3b). As the simulation proceeds, the errors that develop at the lateral boundary appear as inward-propagating waves, and these erroneously generated waves grow until (1) is no longer applicable. When the inward-propagating waves reach sufficient amplitude, the local calculation of the phase speed becomes essentially meaningless.

3. Two-layer shallow-water flow

The preceding examples demonstrate the difficulty of implementing Orlanski-style boundary conditions in the one-dimensional shallow-water system. These results are discouraging since the one-dimensional shallow-water system is one of the few situations where there is a true wave speed that might be calculable from (2). On the other hand, the one-dimensional shallow-water system is also one of the few systems in which there is no need for the Orlanski approach, because it is easy to specify c^*. In systems that support waves moving at different speeds, it is not possible to specify a unique c^*, and it may be more effective to calculate some (presumably averaged) c^* via (2) than to fix c_a at a constant value. This possibility may be examined by considering the case of linearized two-layer shallow-water flow parallel to the x axis, which is governed by the following system of equations (Gill 1982, p. 119):

[3] There are 12 grid points per wavelength in the dominant disturbance in this test case. Higher resolution further improves the c^* calculation shown in Fig. 3b.

$$\frac{\partial u_1}{\partial t} + g\frac{\partial h_1}{\partial x} = 0, \quad (11)$$

$$\frac{\partial u_2}{\partial t} + g\frac{\rho_1}{\rho_2}\frac{\partial h_1}{\partial x} + g'\frac{\partial h_2}{\partial x} = 0, \quad (12)$$

$$\frac{\partial h_1}{\partial t} + H_1\frac{\partial u_1}{\partial x} + H_2\frac{\partial u_2}{\partial x} = 0, \quad (13)$$

$$\frac{\partial h_2}{\partial t} + H_2\frac{\partial u_2}{\partial x} = 0, \quad (14)$$

where $g' = g(\rho_2 - \rho_1)/\rho_2$, and u, ρ, h, and H denote the perturbation horizontal velocity, the density, the elevation of the top of each layer, and the mean depth of each layer. The subscripts 1 and 2 indicate quantities in the upper and lower layer, respectively. This system supports two different modes (one external and one internal wave) that move at speeds

$$c = \pm\left(\frac{gH_1}{1-\mu}\right)^{1/2}, \quad (15)$$

where μ is one of the two roots of

$$\mu^2 + \frac{gH_2 + gH_1 - 2g'H_2}{g'H_2}\mu + \frac{g'H_1 - gH_2}{g'H_1} = 0. \quad (16)$$

Numerical solutions were computed for two-layer flow using forward–backward differencing and spatial and temporal discretizations similar to those in the one-layer case. Three cases were considered; in all three $H_1/H_2 = 1$. In case A, $g' = 0.85g$ and the phase speeds of the two waves, 82.4 and 54.8 m s^{-1}, are close together. In case B, $g' = 0.2g$ and the phase speeds, 96.3 and 22.7 m s^{-1}, are more widely separated. Case C is an intermediate situation for which $g' = 0.5g$ and the phase speeds are 91.4 and 37.9 m s^{-1}. In all cases, the horizontal structure of the initial disturbance is described by (7) and the vertical structure is chosen to equally partition the total perturbation energy between the two modes. The cumulative boundary-induced error in the two-layer system is computed as

$$E_2 = \frac{1}{4N_t}\sum_{n=1}^{N_t}\sum_{k=1}^{2}\sigma_{u_k}(n) + \sigma_{h_k}(n), \quad (17)$$

where, as before, $\sigma_\phi(n)$ is computed from (10).

Figure 4 shows the cumulative boundary-induced error in simulations of cases A and B with c^* fixed at c_a or with c^* calculated using the Orlanski-type formula (8). Not surprisingly, the fixed c_a method and the Orlanski-type procedure both work best in case A, the case with the least difference in the speed of the fastest and the slowest mode. Of more significance is the fact that, for a wide range of c_a, the fixed c^* scheme is superior to the scheme in which c^* is computed at the boundary using (8). Indeed, the range of c_a over which the fixed-c^* approach is superior is larger than in the one-layer case (compare with Fig. 2). According to

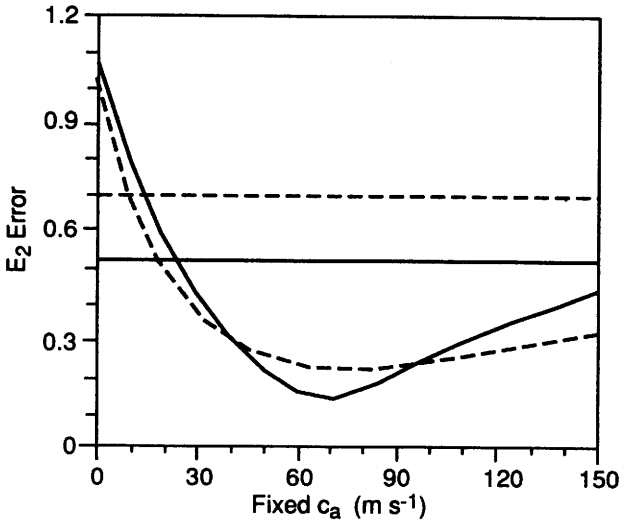

FIG. 4. Cumulative boundary-induced error after 500 time steps (E_2) as a function of c_a for cases A (two modes moving at somewhat similar speeds, solid line) and B (modes moving at very different speeds, dashed line). Also shown are the results from the Orlanski method (8), for which case A is the solid straight line and case B is the dashed straight line.

Fig. 4, in case A, the optimal value of c_a is approximately the average of the speeds of the fast and slow modes. In case B, however, the optimal c_a is closer to the speed of the fast mode. In both cases, good results could have been obtained by fixing c_a at the phase speed of the fast mode. Although the current problem is considerably less complex, these results support the idea that, in simulations of continuously stratified flow, a good choice for a fixed value of c^* is the phase speed of the most rapidly moving internal gravity wave NH/π (Klemp and Wilhelmson 1978). Here N is the Brunt–Väisälä frequency, H is the depth of the model domain, and the longest vertical wavelength excited to significant amplitude is assumed to be $2H$.

One strategy for improving the calculation of c^* is to temporally or spatially smooth the result of (8) (Durran and Klemp 1983). Figure 5 (solid line) shows the result of smoothing the rapid time variations in the c^* calculation with a running time filter

$$c_s^*(n) = \alpha c_s^*(n-1) + (1-\alpha)c^*(n), \quad (18)$$

where $c_s^*(n)$ represents the time-smoothed phase speed at time step n. The results shown in Fig. 5 are for case C, in which the difference in wave speeds is intermediate between those in cases A and B. The initial value of c^* was set to 70 m s^{-1}, which is a nearly optimal value of c_a for use with the fixed-c^* approach. As indicated in Fig. 5, the best results are obtained for $\alpha = 1$, which corresponds to fixing c^* at its initial value of 70 m s^{-1}. The E_2 error is significantly larger for $0 \leq \alpha \leq 0.9$. Figure 5 also shows the effects of both temporally and spatially smoothing the c^* calculation

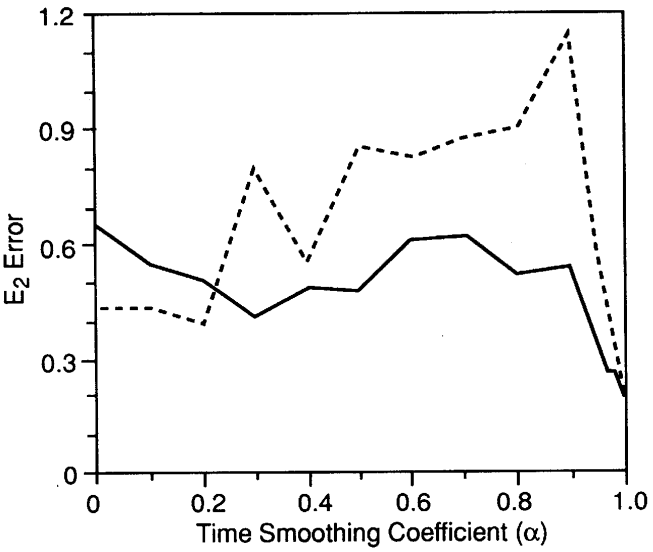

FIG. 5. Cumulative boundary-induced error after 500 time steps (E_2) as a function of the running-time smoothing coefficient α with (dashed line) and without (solid line) vertical averaging of c^*.

(dashed line). Spatial smoothing was performed by averaging the c^* computed for u_1 and u_2 together. Spatial smoothing slightly reduced the error when α was small, and increased it when α was large. The best results were, nevertheless, obtained for $\alpha = 1$ or, equivalently, for fixed c^*.

Some idea of the spatial distribution of the error in a representative two-layer solution is provided by Fig. 6, which shows the large-domain periodic solution, an Orlanski-type solution (with $\alpha = 0.2$ and no spatial averaging of c^*), and a solution with c^* fixed at $c_a = 70$ m s^{-1}. Numerical solutions are plotted for both the free surface (h_1, upper curves) and the internal interface (h_2, lower curves). Figure 6 shows both the limited domain (the unshaded region $0 \leq x \leq 4$ km) and the left-hand portion of the outer periodic domain (the shaded region $-8 \leq x \leq 0$ km). The portion of the outer periodic domain is shown to illustrate the nature of this wave-propagation problem. The four peaks that comprise the faster-moving, external mode (interface displacements smaller than and in phase with the free surface) have almost separated from the four peaks of the slower-moving, internal mode (interface displacements greater than and 180° out of phase with the free surface). The last crest of the internal mode is just reaching the boundary. As evident from the solutions within the shaded region of Fig. 6, large errors are generated in the Orlanski-type solution. The constant-c^* solution performs significantly better, although it still introduces serious error in h_2.

4. An application of the Engquist and Majda method

In atmospheric applications it is common to assume that the difficulties associated with the specification of c^* arise from our interest in dispersive waves. In fact, (1) does not adequately describe the radiation of nondispersive waves in multidimensional systems. A simple example of the problem, and one promising technique for the construction of more accurate wave-permeable boundary conditions, may be illustrated by examining two-dimensional shallow-water flow.

In the case of zero mean flow, the linearized shallow-water equations reduce to (4). For wave solutions of the form

$$\phi(x, y, t) = \phi_0 \exp[i(kx + ly - \omega t)] \quad (19)$$

(here k and l may be positive or negative, but $\omega > 0$ to avoid redundancy), the shallow-water dispersion relation becomes

$$\omega^2 = c^2(k^2 + l^2), \quad (20)$$

or equivalently

$$k = \pm \frac{\omega}{c}\left(1 - \frac{c^2 l^2}{\omega^2}\right)^{1/2}. \quad (21)$$

The group velocity parallel to the x axis is

$$c_{g_x} = \frac{\partial \omega}{\partial k} = kc(k^2 + l^2)^{-1/2}. \quad (22)$$

No plus or minus sign appears in (22) because the sign of the group velocity is determined by the sign of k.

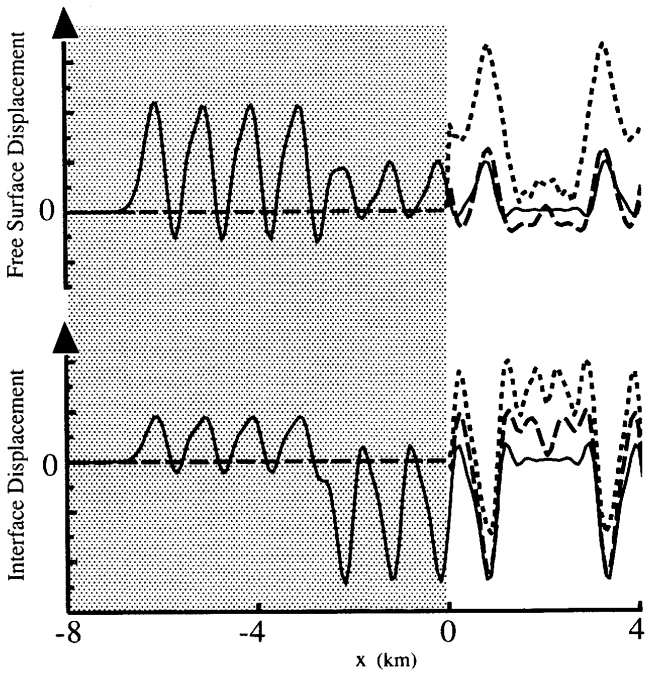

FIG. 6. Free-surface (upper curves) and interface displacements (lower curves) for three solutions to the two-layer problem. Periodic large-domain solution (solid line), limited-domain solutions with constant c^* (long-dashed line), and c^* computed from Orlanski's formula (8) (short-dashed line). Both the limited domain ($0 \leq x \leq 4$ km) and the left half of the extended periodic domain (shaded region $-8 \leq x \leq 0$ km) are shown. The Orlanski and constant c^* solutions are computed only within the limited domain.

Spurious reflection at the right-hand boundary can be eliminated by requiring that all waves at the boundary propagate energy in the positive x direction, or equivalently, that their dispersion relation is given by the positive root of (21). Thus, the x trace velocity for rightward-moving waves is

$$\frac{\omega}{k} = c\left(1 - \frac{c^2 l^2}{\omega^2}\right)^{-1/2}, \tag{23}$$

and if the one-dimensional radiation condition (1) is used to transmit two-dimensional shallow-water waves, c^* must be

$$c^* = c\left(1 - \frac{c^2 l^2}{\omega^2}\right)^{-1/2}, \tag{24}$$

which is a function of both the frequency and the wavenumber parallel to the boundary.

One could attempt to estimate c^* locally using the basic Orlanski formula (2). As shown in section 2, this approach does not work particularly well in one spatial dimension, and it does even worse in two-dimensional flow. Raymond and Kuo (1984) attempted to improve the performance of the Orlanski scheme in two-dimensional problems by generalizing the radiation condition to (3) and calculating the x- and y-component phase speeds as

$$c_x^* = -\frac{\partial\phi}{\partial t}\frac{\partial\phi}{\partial x}\left[\left(\frac{\partial\phi}{\partial x}\right)^2 + \left(\frac{\partial\phi}{\partial y}\right)^2\right]^{-1},$$

$$c_y^* = -\frac{\partial\phi}{\partial t}\frac{\partial\phi}{\partial y}\left[\left(\frac{\partial\phi}{\partial x}\right)^2 + \left(\frac{\partial\phi}{\partial y}\right)^2\right]^{-1}. \tag{25}$$

These formulas reduce to the standard Orlanski scheme if the gradient in ϕ parallel to the boundary is zero.

Engquist and Majda (1977) proposed an alternative approach, based on the concept of one-way wave equations. Under the assumption that $c^2 l^2/\omega^2$ was small, they constructed a series of progressively more accurate approximations to the positive root of (21). Each approximate dispersion relation was associated with a partial differential equation that could be integrated using finite differences computable at the boundary. The lowest-order approximation completely neglects the $c^2 l^2/\omega^2$ term in the square root in (21). This is formally correct only when the wave fronts are perpendicular to the boundary, that is, when the flow is one-dimensional. The resulting dispersion relation ($\omega = ck$) is associated with the differential equation

$$\frac{\partial\phi}{\partial t} + c\frac{\partial\phi}{\partial x} = 0, \tag{26}$$

which is identical to the radiation condition for one-dimensional flow. Engquist and Majda's higher-order approximations remain accurate for larger values of $c^2 l^2/\omega^2 = l^2/(k^2 + l^2)$, that is, for waves that strike the boundary at progressively more acute angles. Their second-order approximation is

$$\left(1 - \frac{c^2 l^2}{\omega^2}\right)^{1/2} \approx 1 - \frac{c^2 l^2}{2\omega^2}, \tag{27}$$

which yields a dispersion relation for rightward-moving waves,

$$\omega^2 - ck\omega - \frac{c^2 l^2}{2} = 0, \tag{28}$$

that is associated with the partial differential equation

$$\frac{\partial^2\phi}{\partial t^2} + c\frac{\partial^2\phi}{\partial t\partial x} - \frac{c^2}{2}\frac{\partial^2\phi}{\partial y^2} = 0. \tag{29}$$

Trefethen and Halpern (1986) have recently proved that (29) is a well-posed boundary condition for the shallow-water equations. The one-way wave equations of Engquist and Majda have been used as boundary conditions in the numerical simulation of acoustic (Halpern and Trefethen 1988) and electromagnetic (Blaschak and Kriegsmann 1988) waves and have been used to evaluate the time dependence in a radiation upper boundary condition for large-scale atmospheric waves (Rasch 1986), but these equations do not seem to have been employed to simulate systems with significant mean flow through the boundary. Engquist and Majda (1977) did consider the shallow-water problem with nonzero mean flow in their original paper, but their formulation relied on a transformation of the dependent variables that has not been widely implemented in practical problems. In the following, we pursue a different approach in which approximate one-way wave equations are constructed for direct application to the standard form of the shallow-water equations.

Consider, therefore, a situation in which there is a mean flow U parallel to the x axis. (Formulas for the general case of mean flow along both the x and y coordinates are presented in the Appendix.) The shallow-water dispersion relation becomes

$$(\omega - Uk)^2 = c^2(k^2 + l^2). \tag{30}$$

Solving for k yields

$$k = \omega\left\{\frac{U \pm c[1 + (l^2/\omega^2)(U^2 - c^2)]^{1/2}}{U^2 - c^2}\right\}. \tag{31}$$

Approximating the square root in the same manner as (27), one obtains the one-way dispersion relations

$$k = \frac{\omega}{U \pm c} \mp \frac{cl^2}{2\omega}, \tag{32}$$

or equivalently, the partial differential equations

$$\frac{\partial^2\phi}{\partial t^2} + (U \pm c)\left(\frac{\partial^2\phi}{\partial t\partial x} \mp \frac{c}{2}\frac{\partial^2\phi}{\partial y^2}\right) = 0. \tag{33}$$

In both (32) and (33) the top set of signs should be used at the right x boundary, and the bottom set at the left boundary. Boundary conditions at the y boundaries

are obtained by solving (30) for l and making the approximation

$$\left[1 - \frac{c^2k^2}{(\omega - Uk)^2}\right]^{1/2} \approx 1 - \frac{c^2k^2}{2(\omega - Uk)^2}, \quad (34)$$

which leads to the one-way dispersion relations

$$l = \pm\left[\frac{\omega - Uk}{c} - \frac{ck^2}{2(\omega - Uk)}\right], \quad (35)$$

and the partial differential equations

$$\left(\frac{\partial}{\partial t} + U\frac{\partial}{\partial x}\right)\left(\frac{\partial}{\partial t} + U\frac{\partial}{\partial x} \pm c\frac{\partial}{\partial y}\right)\phi - \frac{c^2}{2}\frac{\partial^2\phi}{\partial x^2} = 0. \quad (36)$$

In (35) and (36), the plus sign should be used at the north y boundary, and the negative sign at the south boundary.

Both (33) and (36) are truly one-way wave equations since, with the appropriate choice of sign, all wave solutions to these equations have group velocities directed outward through the boundaries. In the case of (33) this is both fortunate and somewhat surprising since the unapproximated equations do not possess this property unless $U = 0$. The x component of the group velocity of a true shallow-water wave is

$$\frac{\partial\omega}{\partial k} = U \pm \frac{ck}{(k^2 + l^2)^{1/2}}. \quad (37)$$

Even when the flow is subcritical ($c > |U|$), the choice of the positive sign in (37) will not ensure that all waves transport energy in the positive x direction. When $U < 0$ and k is sufficiently less than l (i.e., when wave propagation is sufficiently parallel to the y axis), the group velocity is negative, independent of the choice of sign. In contrast, the dispersion relation (32) is associated with x-component group velocities

$$\frac{\partial\omega}{\partial k} = \frac{\omega(U \pm c)}{2\omega - (U \pm c)k}, \quad (38)$$

or substituting for k from (32)

$$\frac{\partial\omega}{\partial k} = \frac{\omega^2(U \pm c)}{\omega^2 \pm cl^2(U \pm c)/2}. \quad (39)$$

If the flow is subcritical, the denominator is always positive and the sign of the group velocity is determined by the choice of sign in the numerator. Thus, if the positive signs are chosen, (33) will require that all waves present at the right x boundary propagate energy outward through the boundary. The y-component group velocities associated with (35) and (36) may be written

$$\frac{\partial\omega}{\partial l} = \pm\frac{c(\omega - Uk)^2}{(\omega - Uk)^2 + c^2k^2/2}, \quad (40)$$

the direction of which is always outward, as determined by the choice of sign in (35). Although no formal proof of the well posedness of (33) and (36) will be provided in this paper, Trefethen's (1983) group velocity interpretation of the Gustafsson–Kreiss–Sundström stability theorem (Gustafsson 1972) suggests that since these conditions require outward-directed group velocities at the boundary there is a reasonable likelihood that they are well posed.

5. Test results for two-dimensional shallow-water flow

In the remainder of this section, the Engquist and Majda scheme will be compared with the Raymond and Kuo scheme and with several other alternative formulations for wave-permeable boundary conditions. In each instance, the finite-difference equations used in the interior of the domain are the two-dimensional generalization of (5) and (6),

$$\delta_{2t}u^n_{i+1/2,j} + U\delta_{2x}u^n_{i+1/2,j} + \delta_x\eta^{n-1}_{i+1/2,j} = 0, \quad (41)$$

$$\delta_{2t}v^n_{i,j+1/2} + U\delta_{2x}v^n_{i,j+1/2} + \delta_y\eta^{n-1}_{i,j+1/2} = 0, \quad (42)$$

$$\delta_{2t}\eta^n_{i,j} + U\delta_{2x}\eta^n_{i,j} + c^2(\delta_x u^{n+1}_{i,j} + \delta_y v^{n+1}_{i,j}) = 0, \quad (43)$$

where the finite-difference operator δ acting on an arbitrary function r is defined as

$$\delta_{nx}r(x_i) = \frac{r(x_i + n\Delta x/2) - r(x_i - n\Delta x/2)}{n\Delta x}. \quad (44)$$

The finite-difference approximations for the Raymond and Kuo boundary conditions, (3) and (25), are specified following Eqs. (9) and (11) of Raymond and Kuo (1984).

In the second-order Engquist and Majda scheme, the one-way wave equation at the right-hand x boundary [(33) with the plus signs] is discretized as

$$\overline{\delta_t^2\phi^n_{b-1/2,j}}^{x} + (U + c)\delta_{2t}\delta_x\phi^n_{b-1/2,j} - \frac{c}{2}(U + c)\overline{\delta_y^2\phi^n_{b-1/2,j}}^{x,2t} = 0, \quad (45)$$

where b is the i index at the boundary, and an averaging operator is defined such that

$$\overline{r(x_i)}^{nx} = \frac{r(x_i + n\Delta x/2) + r(x_i - n\Delta x/2)}{2} \quad (46)$$

and

$$\overline{r(x_i, y_j)}^{nx,ny} = \left[\overline{r(x_i, y_i)}^{nx}\right]^{ny}. \quad (47)$$

At the "upper" y boundary (36) becomes

$$\overline{\delta_t^2\phi^n_{i,b-1/2}}^{y} + 2U\overline{\delta_{2t}\delta_{2x}\phi^n_{i,b-1/2}}^{y} + c\delta_{2t}\delta_y\phi^n_{i,b-1/2} + (U^2 - c^2/2)\overline{\delta_x^2\phi^n_{i,b-1/2}}^{y,2t} + Uc\overline{\delta_{2x}\delta_y\phi^n_{i,b-1/2}}^{2t} = 0. \quad (48)$$

The interior solution is updated first; then (45) and (48) are solved at the boundary. The implicit coupling

in these equations requires the solution of a tridiagonal system at each boundary. These boundary conditions are applied separately to u, v, and η. The Engquist and Majda scheme requires special formulas near the corner points. The actual corner points are not used in the integration; they are filled in by interpolation for cosmetic purposes. The boundary points directly adjacent to a true corner were computed using the first-order one-way wave equation (26), with c replaced by the appropriate Doppler-shifted value, $U \pm c$, at the x boundaries. The first-order formula avoids the difficulty of computing second derivatives parallel to the boundary in the vicinity of the corners.

Four other wave-permeable boundary conditions were also considered: the first-order Engquist and Majda scheme, the Rayleigh damping sponge layer of Davies (1983), and two mixed approaches that will be referred to as the "zero-gradient" and "fixed-inflow" schemes. The boundary conditions imposed in each test case are listed in Table 1. In the first-order Engquist and Majda method (EM1), the appropriately Doppler-shifted variant of (26) is imposed for all variables at all boundaries using upstream differencing. In the zero-gradient scheme (ZG), the Doppler-shifted version of (26) is applied only to the normal velocity. The boundary values of the height field and the tangential velocity, which are specified at locations one-half grid interval inside the actual edge of the computational domain due to the grid staggering, are computed from the full governing equations—except that the advection perpendicular to the boundary is evaluated using one-sided differences at outflow and set to zero at inflow. The fixed-inflow scheme (FI) is identical to the zero-gradient scheme except that the height field and tangential velocity are fixed at inflow. (Note that since it is computed using the first-order Enquist and Majda method, the normal velocity is not fixed at inflow by the FI scheme.) Both the FI and the ZG schemes are the shallow-water analogs to procedures currently used in many mesoscale atmospheric models.

The sixth and final approach is the tendency modification scheme of Davies (1983), in which an eight-point Rayleigh damping sponge layer is appended to each edge of the domain (DSP). Within the sponge, an intermediate result $\hat{\phi}_i^{n+1}$ was first computed using the full equations. The final result ϕ_i^{n+1} was then calculated as

$$\phi_i^{n+1} = \hat{\phi}_i^{n+1} - \gamma_i(\hat{\phi}_i^{n+1} - \phi_b). \quad (49)$$

Here ϕ_b is the fixed boundary value, i is the coordinate index in the direction normal to the boundary, and γ_i assumes the values 0.02, 0.1, 0.25, 0.5, 0.75, 0.9, 0.98, and 1.0 as i approaches the outside edge of the sponge layer.[4]

[4] The values of γ_i given above are for the tangential velocity and the height fields. The γ_i for the normal velocity were interpolated between these values to account for the mesh staggering.

TABLE 1. Summary of the boundary conditions employed in the two-dimensional shallow-water simulations.

EM1	First-order Engquist and Majda scheme applied to all fields.
EM2	Second-order Engquist and Majda scheme applied to all fields.
FI	First-order Engquist and Majda scheme applied to normal velocities. Height and tangential velocities fixed at inflow. Height and tangential velocities computed using upstream differencing at outflow.
ZG	As in FI except that the gradient in the height and tangential velocities is zero at inflow.
RK	Raymond and Kuo scheme applied to all fields.
DSP	Eight-point Rayleigh damping sponge applied to all fields.

In the following simulations, three of the preceding methods, the Raymond and Kuo, the second-order Engquist and Majda, and the sponge-layer, gradually generate short-wavelength noise near the boundary. The finite-difference scheme used in these tests is completely nondissipative, so it permits the noise to accumulate until (particularly in the Raymond and Kuo method) it reaches unacceptable levels. Thus, when integrating with the Raymond and Kuo, the second-order Engquist and Majda, and the sponge-layer boundary conditions, a second-order smoother of the form

$$\phi_{i,j}^{n+1} = \tilde{\phi}_{i,j}^{n+1} + \alpha\Delta t(\delta_x^2\phi_{i,j}^{n-1} + \delta_y^2\phi_{i,j}^{n-1}), \quad (50)$$

where $\tilde{\phi}$ denotes a spatially unsmoothed variable, was employed in a *four-gridpoint-wide strip* adjacent to each boundary. The computations at the other interior points were not smoothed. The smoothing coefficient was $\alpha/\Delta x^2 = 0.016$.

These methods are compared in a series of simulations of shallow-water flow over topography. The topography is an isolated circular mountain of the form

$$z_s(x, y) = h_0\left(\frac{x^2 + y^2}{a^2} + 1\right)^{-3/2}, \quad (51)$$

where $a = 5$ km and h_0 is 10% of the total fluid depth, which is chosen such that $c = \sqrt{gH} = 40$ m s^{-1}. The mean flow is 10 m s^{-1} parallel to the x axis. The U and c employed in the Engquist and Majda boundary conditions were, therefore, 10 and 40 m s^{-1}. The horizontal resolution is 1 km along both coordinate axes; the time step is 5.657 s. The initial conditions for each simulation are $\eta = u = v = 0$, and these values define the fixed-height and tangential-velocity fields at the inflow boundaries in the FI simulation. The computational domain consisted of the rectangular region -20 km $\leq x \leq 20$ km, -40 km $\leq y \leq 40$ km. The wide domain in the direction parallel to the y axis allows a clear examination of the transients generated by the impulsive start as they propagate through the lateral boundary at a nonnormal angle of incidence.

As the flow adjusts to the presence of the mountain, a semicircular wave of elevation propagates upstream; a semicircular wave of depression propagates down-

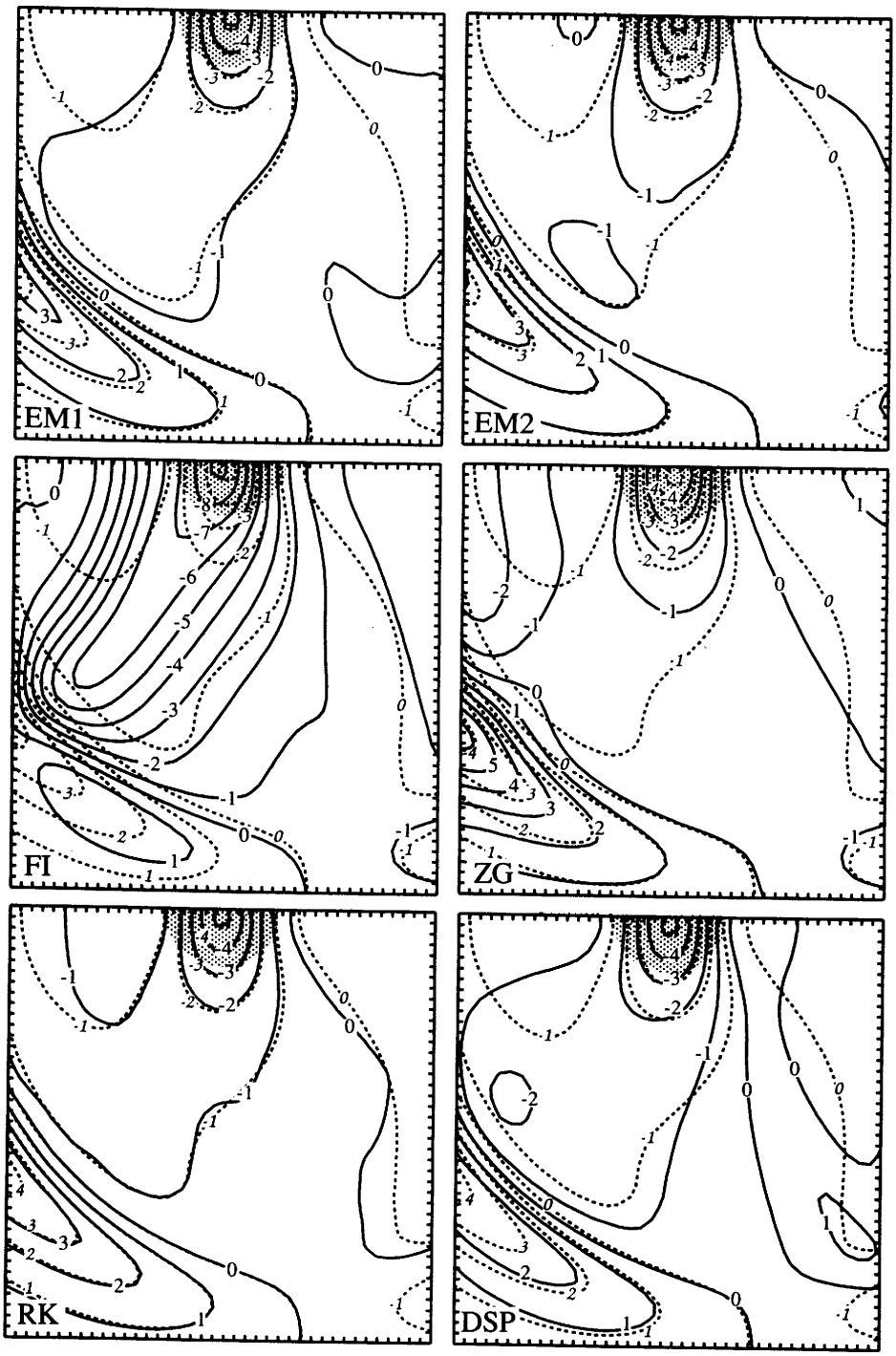

FIG. 7. Height contours of the free surface at $ct/a = 7.25$ after the impulsive start. Only the lower half of the domain is shown; the solution is symmetric about the top boundary. The region where the topography is higher than $h_0/2$ is shaded. Dashed contours are the large-domain solution; solid contours are solutions generated using the following boundary conditions: first-order Engquist and Majda (EM1); second-order Engquist and Majda (EM2); first-order Engquist and Majda for the normal velocities and the other fields fixed at inflow and upstream differenced at outflow (FI); as in FI with a zero gradient specified for the nonnormal velocity and the height field at inflow (ZG); Raymond and Kuo (RK); and an eight-gridpoint Davies sponge layer (DSP).

stream, and a wave of depression remains above the mountain. The height field at $ct/a = 7.25$ is contoured for all six solutions in Fig. 7 (solid lines). Each solution is compared with a control simulation computed on a much larger (400 km × 400 km) mesh (dashed lines). Only the bottom half of the domain is shown in Fig.

7. The u and η fields are symmetric about the top edge of the domain; v is antisymmetric. The shaded half-circle at the top of each panel indicates the region where the mountain height is greater than $h_0/2$. The transient wave of elevation appears as the prominent arc in the lower left of each panel. The Raymond and Kuo and second-order Engquist and Majda schemes both pass this wave through the boundary with a minimum of distortion. The first-order Engquist and Majda and the sponge-layer schemes produce substantially more error, but even these schemes look good compared to the ZG and FI methods. The ZG method amplifies the outgoing wave and produces a spurious region of depressed heights directly upstream of the mountain. The worst results are, however, obtained using the FI method that generates a very strong reflected wave.

The downstream-propagating wave of depression, which has almost left the domain by the time shown in Fig. 7, is visible as the small region of -1 heights in the lower-right corner of the domain. Data from earlier times in the simulation (not shown) indicate that the Raymond and Kuo, second-order Engquist and Majda, ZG and FI schemes all do a superior job of modeling the downstream-propagating wave. The first-order Engquist and Majda and the sponge-layer methods generate significantly larger errors during the passage of the downstream-propagating wave. The dramatic difference between the treatment of the upstream- and downstream-propagating waves by the ZG and FI methods arises because these methods closely approximate the governing equations with one-sided differencing at outflow boundaries but use crude assumptions about v and η at inflow.

Although it is certainly important for wave-permeable boundary conditions to pass transient disturbances through the boundary with minimal distortion of the transient, good wave-permeable boundaries must also correctly represent the influence of the boundaries on the steady-state-forced solution. Some indication of the influence of the lateral boundaries on the forced solution may be obtained from Fig. 7, in which it appears that all methods, except the ZG and FI schemes do a similar and satisfactory job of representing the disturbance above the mountain. The subtle influences of the lateral boundary conditions on the steady solution are more clearly revealed by examining the fields at $ct/a = 14.5$, by which time the solutions are nearly at steady state. Figure 8 shows the steady-state height field for all six solutions. The best results are obtained with the second-order Engquist and Majda scheme. The worst results are produced by the Raymond and Kuo method. The FI and ZG methods also perform poorly. The error patterns in the u and v fields are somewhat different from those in the height field and are shown in Figs. 9 and 10.

Contours of v are compared with those for the wide-domain simulation in Fig. 9. The second-order Engquist and Majda solution is clearly the best. Significant errors occur over the upstream side of the mountain in all the other methods. (Note that both the first-order Engquist and Majda and the ZG schemes are almost one contour interval in error, so that the results for those methods are much worse than they may appear at first glance.) The sponge-layer and Raymond and Kuo methods also exhibit short-wavelength noise near the downstream boundary that is too strongly forced to be completely eliminated by the limited diffusion in the four-point smoothing strip adjacent to the boundary. The u field is compared with the large domain solution in Fig. 10. The FI and ZG schemes are the worst; both produce large and spurious velocity perturbations upstream of the mountain. In contrast to the situation with the η and v fields, however, the second-order Engquist and Majda u field is not clearly superior to the results obtained with the first-order Engquist and Majda method or the sponge-layer scheme. Indeed, the second-order Engquist and Majda result is somewhat inferior in the region over and "south" of the mountain, although it does do a better job near the upstream and downstream boundaries.

An idea of the time-dependent behavior of the combined boundary-induced error in u, v, and η is provided in Fig. 11, which shows the total error

$$E(t) = \frac{1}{3N_t(t)} \sum_{n=1}^{N_t} [\sigma_u(n) + \sigma_v(n) + \sigma_h(n)], \quad (52)$$

where $N_t(t)$ is the number of time steps required to advance the solution to time t and, as in one-dimensional tests, $\sigma_\phi(n)$ is computed from (10). Consistent with the results shown in Fig. 7, the second-order Engquist and Majda and the Raymond and Kuo schemes are the best at early times. The error in the Raymond and Kuo scheme increases rapidly after $N_t = 160$, and after this time, the second-order Engquist and Majda scheme is the best. The boundary-induced errors do decrease with time after $N_t = 240$ in the sponge-layer method, so that by the end of the simulation the error in the sponge-layer method is competitive with that of the second-order Engquist and Majda scheme. The large decrease in the error produced by the sponge-layer scheme is, however, attributable to the localized and steady-state character of the forced solution and does not occur in problems where transient waves are continually forced in the interior.

In order to examine a case where a series of transient waves impinges on the lateral boundaries, the stationary mountain was replaced by an oscillating lower boundary of the form

$$z_s(x, y, t) = \begin{cases} h_0 \sin(\omega t) \cos^8\left[\dfrac{\pi}{2a}(x^2 + y^2)^{1/2}\right], \\ \qquad\qquad \text{if} \quad x^2 + y^2 \leq a^2; \\ 0, \quad \text{otherwise.} \end{cases} \quad (53)$$

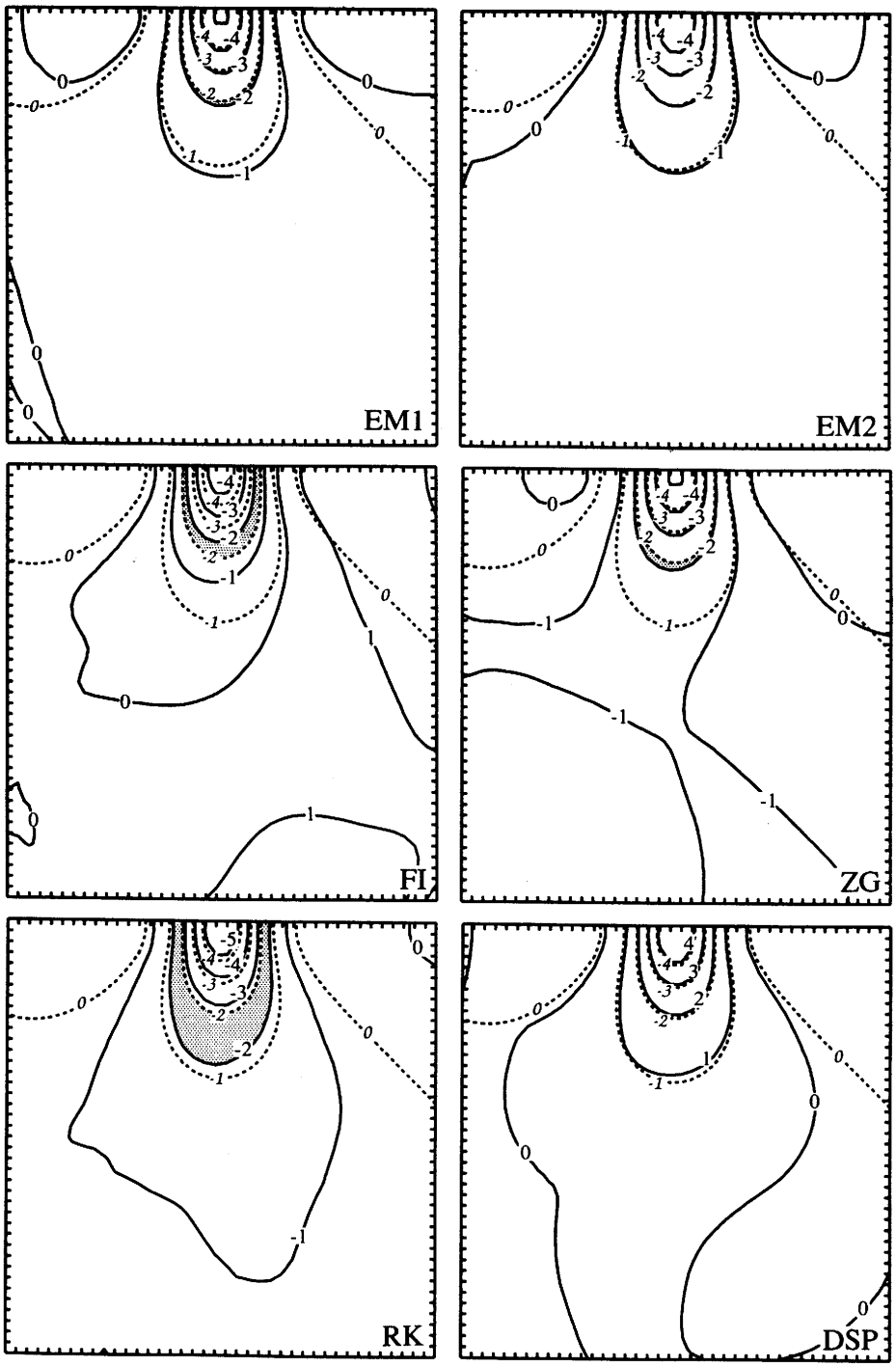

FIG. 8. As in Fig. 7 except at $ct/a = 14.5$ after the impulsive start. The position of the mountain is not indicated, but it is identical to that in Fig. 7. The region between the -2 contours in the large-domain and limited-area solutions is shaded.

The preceding simulations were repeated using this oscillating lower boundary to force waves in a basic state with zero mean wind. All parameters in the oscillating mountain case were the same as in the fixed mountain problem, except that $a = 14.7$ km, $\Delta t = 7.07$ s, $\omega = 2\pi/48\Delta t$, and $U = 0$. The cumulative error $E(t)$ from this simulation is plotted in Fig. 12. The superiority of the second-order Engquist and Majda method is again apparent.

6. Discussion and conclusions

This paper has focused on the numerical simulation of relatively simple wave-propagation problems. The

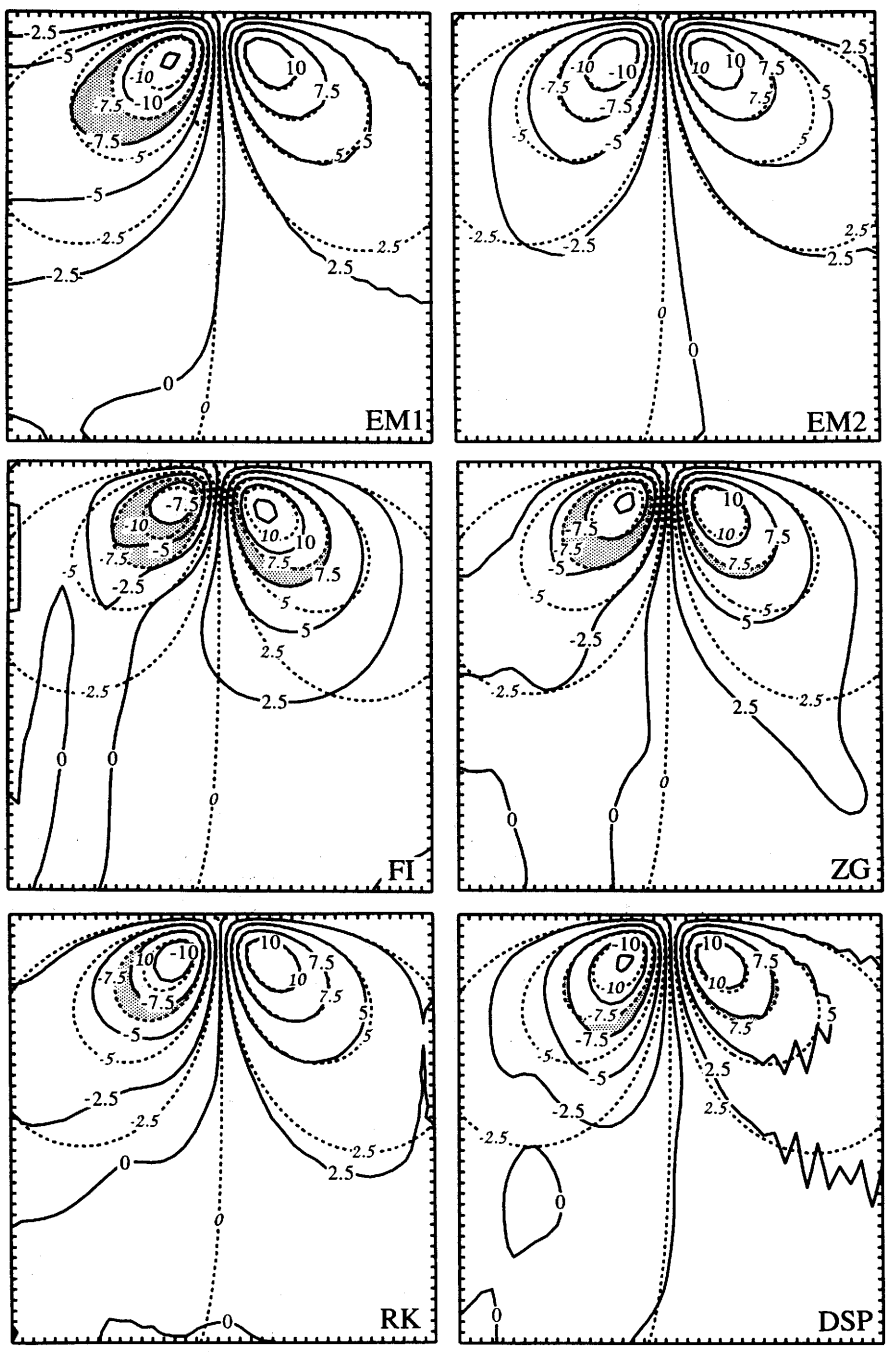

FIG. 9. As in Fig. 8 except that the v field is contoured, and shading indicates the region between the ± 7.5 contours in the large-domain and limited-area solutions.

correct solution to these problems was easy to determine and could, therefore, be used to unambiguously assess the accuracy of several wave-permeable boundary conditions. One-dimensional shallow-water flow was the first case considered. The results of our one-dimensional shallow-water tests indicate it is better to externally specify c^* in the one-way wave equation (1) than to attempt to calculate it using (2). The externally specified c^* could deviate from the true phase speed $U + c$ by 40%–60% and still yield better results than schemes in which c^* was calculated locally from (2). Computations performed using the numerical solution on a large periodic domain demonstrated that, except during the passage of a wave trough or crest, (2) was capable of diagnosing a reasonable approximation to $U + c$ provided that all waves propagating past the

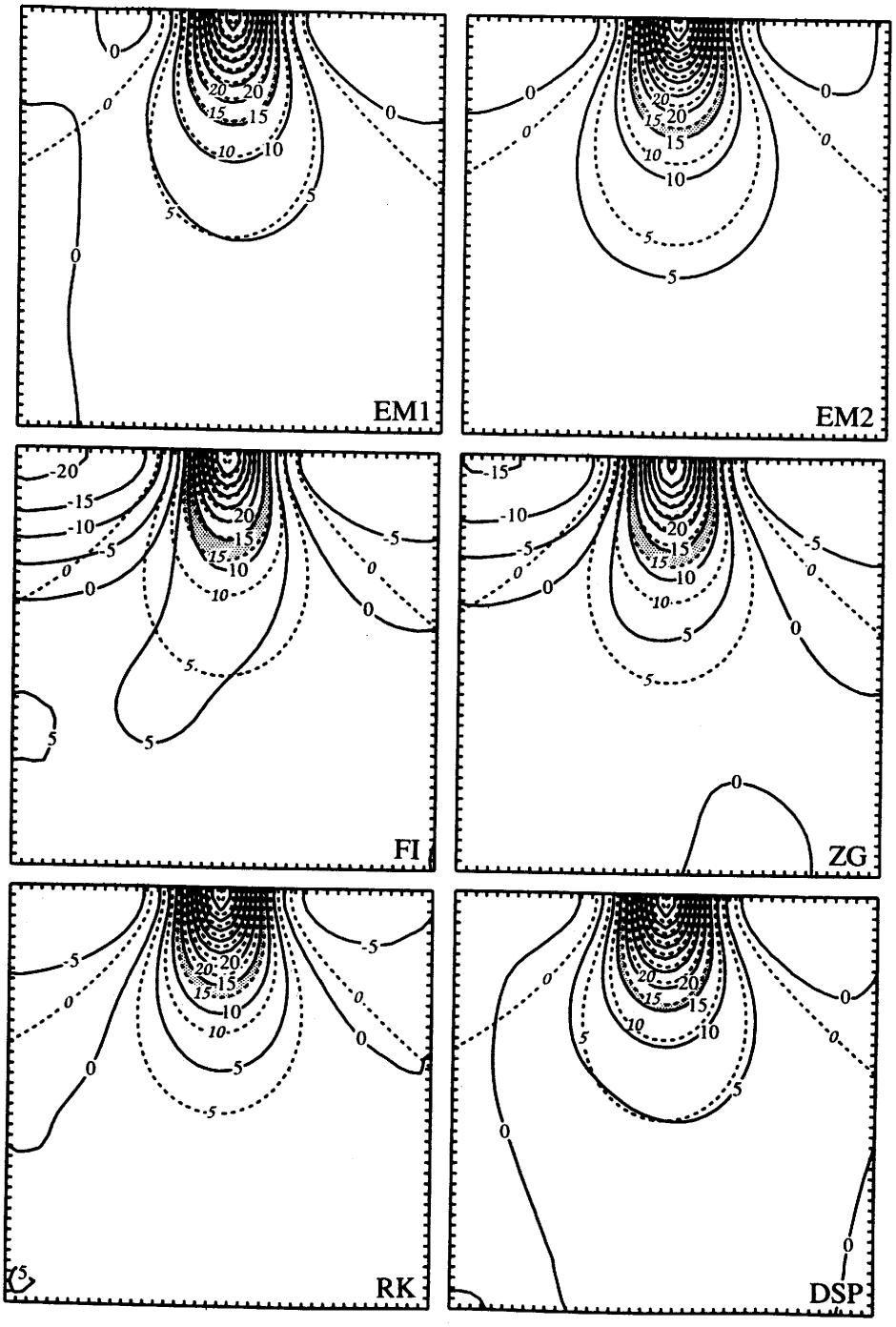

FIG. 10. As in Fig. 9 except that the u field is contoured, and shading indicates the region between the 15 contours in the large-domain and limited-area solutions.

point of calculation were really traveling in the positive x direction. However, when the c^* calculation was attempted at the boundary of a limited domain, small errors in the boundary conditions gave rise to leftward-propagating waves. Although these leftward-propagating waves were initially small, they degraded the local calculation of c^*, since (2) does not apply at locations where both rightward- and leftward-propagating waves are present. The additional error in c^* increased the error at the boundary that amplified the spurious leftward-propagating waves, creating a positive feedback that rapidly destroyed the reliability of the c^* calculation.

The question of whether it is better to specify or calculate c^* was also examined through experimentation with a two-layer shallow-water model. Although the two-layer system is dispersive and waves with different phase speeds were present at the boundary si-

multaneously, our results suggest that, once again, it is better to externally specify some fixed c^* than to calculate c^* at the boundary. In fact, the advantages of specifying a fixed c^* were more pronounced in the two-layer system than in single-layer flow. A reasonable, though not optimal, choice for c^* was the phase-speed of the fastest-moving wave. Attempts to refine the Orlanski-type phase-speed calculation by temporally or spatially smoothing c^* were explored, but these did not yield significant improvement.

Clark (1979) and Hedley and Yau (1988) have suggested that it is better to calculate c^* than to fix it. Our results are not necessarily in conflict with those of Clark, and Hedley and Yau, however, since there is a considerable difference in the nature of the test problems. Their studies examined the difference between large- and small-domain simulations of deep convective clouds. As noted by Clark, the surrounding fluid exerts a feedback on the convection through its "inertia," which resists the spinup of a convergent lower-level inflow and a divergent upper-level outflow. Thus, the boundary condition that best mimics the convection in the larger domain may be one producing a spurious inward-propagating signal that approximates the influence of the surrounding fluid. On the other hand, a true radiation boundary will not communicate signals inward through the boundary, and in such tests, it may not provide the best results. The preceding concerns should not, however, be interpreted as suggesting that radiation boundary conditions are bad for cloud modeling. Provided the computational domain is sufficiently large, the nonlinear feedback of the surrounding fluid on the convective cloud will be very weak, and true radiation boundary conditions should allow the most accurate numerical simulation.

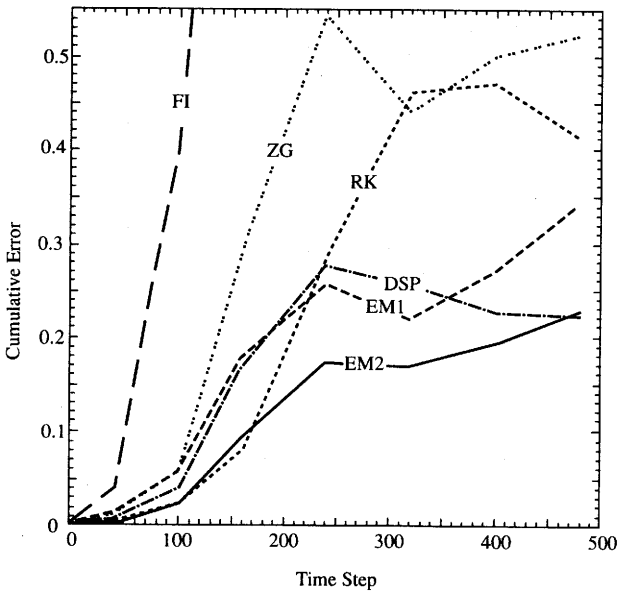

FIG. 11. Cumulative error [see (52)] as a function of time step in shallow-water flow over topography. Curves shown are for the first-order Engquist and Majda method (EM1), the second-order Engquist and Majda method (EM2), the fixed-inflow method (FI), the zero-gradient method (ZG), the Raymond and Kuo method (RK) and Davies' sponge layer (DSP).

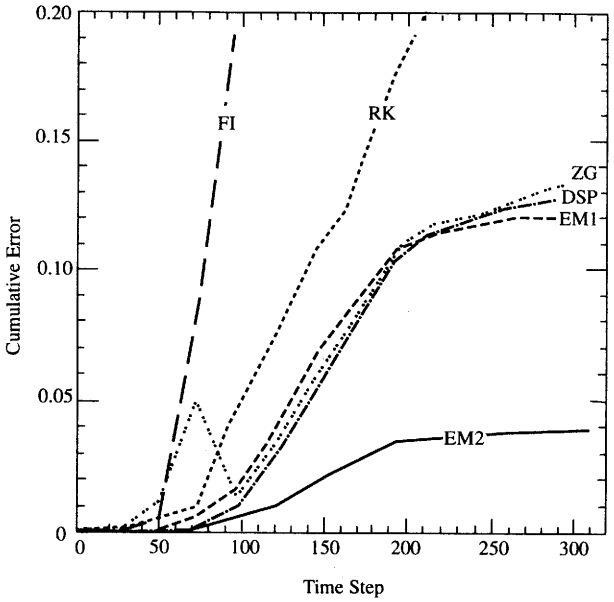

FIG. 12. As in Fig. 11 except the waves are forced by an oscillating lower boundary.

Wave-permeable boundary conditions for two-dimensional shallow-water flow have also been examined in this paper. Although two-dimensional shallow-water waves travel at a known phase speed, the trace velocities along the x and y axes are functions of wavelength and, therefore, (1) provides only an approximate radiation boundary condition for two-dimensional waves. Engquist and Majda (1977) suggested a way to improve the accuracy of (1), but their original formulation does not conveniently generalize to cases with nonzero mean flow. In this paper, the one-way wave equation technique of Engquist and Majda was used to construct new boundary conditions that are easily applied to cases with a mean flow. The well posedness of the new boundary conditions has not been rigorously investigated, but the new conditions do require the group velocity of all waves at the boundary to be directed outward through the boundary, which is essential for well posedness. These boundary conditions have proved stable and accurate in practice. Indeed, they provided the best results in our two-dimensional test cases. In particular, they performed better than the first-order one-way wave equation (1), the method of Raymond and Kuo (1984), the eight-point sponge of Davies (1983), and two hybrid methods.

Many mesoscale models of the atmosphere require open boundary conditions for three-dimensional stratified flow. Although boundary conditions for the full

three-dimensional problem have not been explicitly tested in this paper, the preceding results suggest the following strategy. A fixed c^* could be estimated, perhaps as the phase speed of the most rapidly moving internal gravity wave NH/π. This c^* could replace c in the one-way wave equations (33) and (36) [or more generally (A1) and (A2)], which could then be used as lateral boundary conditions for stratified flow. Future research will be required to evaluate the effectiveness of this procedure in fully three-dimensional mesoscale models.

Acknowledgments. Dale Durran was supported by NSF Grant ATM-8914852. Ming-Jen Yang was supported by NSF Grant ATM-9101653. Donald Slinn was supported by ONR Grant N00014-90-J-1112. Randy Brown was supported by Department of the Air Force Fellowship S-789-000-057.

APPENDIX

Formulas for Mean Flows at Arbitrary Angles

For generalized two-dimensional mean flow, the second-order one-way wave equations at the x boundaries become

$$\frac{\partial^2\phi}{\partial t^2} + (U \pm c)\frac{\partial^2\phi}{\partial t\partial x} + V(U \pm c)\frac{\partial^2\phi}{\partial x\partial y} + 2V\frac{\partial^2\phi}{\partial t\partial y} + \left[V^2 \mp \frac{c}{2}(U \pm c)\right]\frac{\partial^2\phi}{\partial y^2} = 0. \quad \text{(A1)}$$

Here U and V denote the components of the mean flow parallel to the x and y coordinates. The top set of signs should be used at the right x boundary and the bottom set at the left boundary. The expression for the y boundaries, which may be obtained by direct derivation or by interchanging x with y and U with V in (A1), is

$$\frac{\partial^2\phi}{\partial t^2} + (V \pm c)\frac{\partial^2\phi}{\partial t\partial y} + U(V \pm c)\frac{\partial^2\phi}{\partial y\partial x} + 2U\frac{\partial^2\phi}{\partial t\partial x} + \left[U^2 \mp \frac{c}{2}(V \pm c)\right]\frac{\partial^2\phi}{\partial x^2} = 0. \quad \text{(A2)}$$

The top set of signs should be applied at the north y boundary and the bottom set at the south boundary.

The preceding conditions were tested in the circular mountain problem, described in section 5, and performed well regardless of the orientation of the mean flow. The north y boundary condition was discretized as

$$\overline{\delta_t^2\phi^n_{i,b-1/2}}^{y} + (V + c)\delta_{2t}\delta_y\phi^n_{i,b-1/2} + U(V + c)\overline{\delta_{2x}\delta_y\phi^n_{i,b-1/2}}^{2t} + 2U\overline{\delta_{2t}\delta_{2x}\phi^n_{i,b-1/2}}^{y} + [U^2 - c(V + c)/2]\overline{\delta_x^2\phi^n_{i,b-1/2}}^{y,2t} = 0, \quad \text{(A3)}$$

where the subscript b denotes the index of a boundary point. The interior solution was updated first, in which case the implicit coupling in (A3) reduces to a tridiagonal system for the boundary points $\phi^{n+1}_{i,b}$. As in the $V = 0$ case, $\phi^{n+1}_{2,b}$ and $\phi^{n+1}_{b-1,b}$ were calculated using the first-order one-way wave equation, which does not require the computation of derivatives parallel to the boundary.

REFERENCES

Blaschak, J. G., and G. A. Kriegsmann, 1988: A comparative study of absorbing boundary conditions. *J. Comput., Phys.*, **77**, 109–139.

Clark, T. L., 1979: Numerical simulations with a three-dimensional cloud model: Lateral boundary conditions and multicellular severe storm simulations. *J. Atmos. Sci.*, **36**, 2191–2215.

Davies, H. C., 1983: Limitations of some common lateral boundary schemes used in regional NWP models. *Mon. Wea. Rev.*, **111**, 1002–1012.

Durran, D. R., and J. B. Klemp, 1983: A compressible model for the simulation of moist mountain waves. *Mon. Wea. Rev.*, **111**, 2341–2361.

Engquist, B., and A. Majda, 1977: Absorbing boundary conditions for the numerical simulation of waves. *Math. Comput.*, **31**, 629–651.

Fovell, R. G., and Y. Ogura, 1988: Numerical simulation of a midlatitude squall line in two dimensions. *J. Atmos. Sci.*, **45**, 3846–3879.

Gill, A. E., 1982: *Atmosphere-Ocean Dynamics.* Academic Press, 662 pp.

Gustafsson, B., H.-O. Kreiss, and A. Sundström, 1972: Stability theory of difference approximations for initial boundary value problems: II. *Math. Comput.*, **26**, 649–686.

Halpern, L., and L. N. Trefethen, 1988: Wide-angle one-way wave equations. *J. Acoust. Soc. Am.*, **84**, 1397–1404.

Hedley, M., and M. K. Yau, 1988: Radiation boundary conditions in numerical modelling. *Mon. Wea. Rev.*, **116**, 1721–1736.

Klemp, J. B., and D. K. Lilly, 1978: Numerical simulation of hydrostatic mountain waves. *J. Atmos. Sci.*, **35**, 78–107.

——, and R. W. Wilhelmson, 1978: The simulation of three-dimensional convective storm dynamics. *J. Atmos. Sci.*, **35**, 1070–1096.

Mesinger, F. and A. Arakawa, 1976: Numerical Methods Used in Atmospheric Models, Vol. I. GARP Pub. Ser. 17, ICSU/WMO, 64 pp.

Miller, M. J., and A. J. Thorpe, 1981: Radiation conditions for the lateral boundaries of limited-area numerical models. *Quart. J. Roy. Meteor. Soc.*, **107**, 615–628.

Orlanski, I., 1976: A simple boundary condition for unbounded hyperbolic flows. *J. Comput. Phys.*, **21**, 251–269.

Pearson, R. A., 1974: Consistent boundary conditions for numerical models of systems that admit dispersive waves. *J. Atmos. Sci.*, **31**, 1481–1489.

Rasch, P. J., 1986: Towards atmospheres without tops: Absorbing upper boundary conditions for numerical models. *Quart. J. Roy. Meteor. Soc.*, **112**, 1195–1218.

Raymond, W. H., and H. L. Kuo, 1984: A radiation boundary condition for multi-dimensional flows. *Quart. J. Roy. Meteor. Soc.*, **110**, 535–551.

Sommerfeld, A., 1949: *Partial Differential Equations in Physics.* Academic Press, 335 pp.

Trefethen, L. N., 1983: Group velocity interpretation of the stability theory of Gustafsson, Kreiss and Sundström. *J. Comput. Phys.*, **49**, 199–217.

——, and L. Halpern, 1986: Well-posedness of one-way wave equations and absorbing boundary conditions. *Math. Comput.*, **47**, 421–435.